ACS NANO

www.acsnano.org

ARTICLE

Sphere-to-Icosahedron Droplet Shape Transformations in Interfacially Frozen Pickering Emulsions

Alexander V. Butenko,[§] Emery Hsu,[§] Daniel A. Matoz-Fernandez, Lee Shool, Andrew B. Schofield, Daeyeon Lee,* and Eli Sloutskin*

Cite This: https://doi.org/10.1021/acsnano.4c13476

Read Online

ACCESS | Metrics & More | Article Recommendations | Supporting Information

ABSTRACT: Surfactant-stabilized oil-in-water and water-in-oil emulsions, encompassing a wide range of chemical compositions, exhibit remarkable temperature-controlled sphere-to-icosahedron droplet shape transformations. These transformations are controlled by the elasticity and closed-surface topology of a self-assembled interfacial crystalline monolayer. Since many practical emulsions are synergistically costabilized by both surfactants and colloidal particles, we explore the influence of surface-adsorbed hydrophobic and hydrophilic colloidal particles on these shape transformations. We find that these shape transformations persist even at high interfacial colloidal densities, despite the colloids disrupting the molecular interfacial crystal's topology. We employ computer simulations to elucidate the role of colloidal particles in droplet shape control of these widely employed emulsions. Surprisingly, we observe that the particles serve as incompressible inclusions, which do not disrupt the out-of-plane buckling of the interfacial crystal. Our findings demonstrate temperature-control of droplet shape transformations and self-division in emulsions costabilized by colloidal particles and molecular surfactants. The fundamental mechanisms uncovered here may have broad implications for biological systems, enable unexplored strategies for microcargo delivery and release, and inspire unconventional approaches in smart material design.

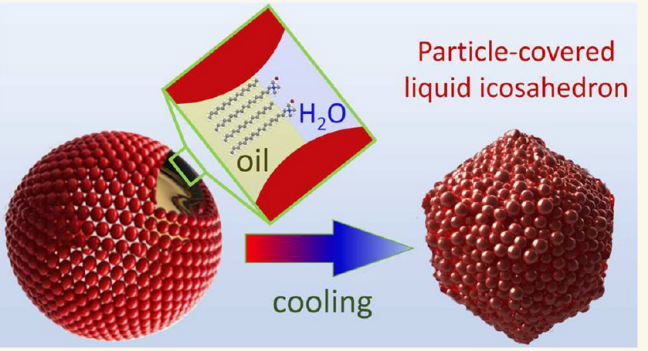

KEYWORDS: *emulsion, self-faceting, self-shaping, topology, Pickering emulsion, geometrical frustration, interfacial freezing*

Oil-in-water emulsions are common in nature and widely employed in food, pharmaceuticals, water treatment, and many other technologies, providing a simple model of biological compartmentalization.[1] Recent studies demonstrate that many surfactant-stabilized emulsions exhibit "interfacial freezing", where a mixed oil:surfactant crystal coexists, over a wide temperature range, with the liquid bulk of the droplet.[2−6] The incompatibility of the hexagonally packed interfacial crystal with the closed-surface topology of the droplets' interfaces leads, according to the celebrated Euler's polyhedron formula,[7] to the formation of 12 "disclination" defects, i.e., lattice sites, where the coordination number is 5 instead of 6.[3] When the interfacial tension $\gamma(T)$ is sufficiently low, these disclinations, possibly decorated by pairs of 5- and 7-coordinated lattice sites,[8−11] induce a sphere-to-icosahedron (S−I) droplet shape transformation,[12,13] forming the 12 vertices of the liquid icosahedral droplets.[2,14−16] This $\gamma(T)$-controlled transformation allows basic properties of the emulsions to be switched reversibly and enables a unique strategy[17] for synthesizing icosahedral building blocks, ranging from tens of μm to tens of nm,[14] for self-assembly of smart metamaterials.[16,18,19]

Previous studies of S−I transformations focused on emulsions where only the *molecular* surfactants were employed for droplets' stabilization against coalescence. To date, no interfacial freezing has been reported for 'Pickering' emulsions−surfactant-free systems stabilized by colloidal particles.[20] However, most common emulsions in nature and technology are synergistically costabilized by both particles and surfactants.[21−24] The impact of particle-surfactant costabiliza-

Received: September 24, 2024
Revised: January 29, 2025
Accepted: January 29, 2025

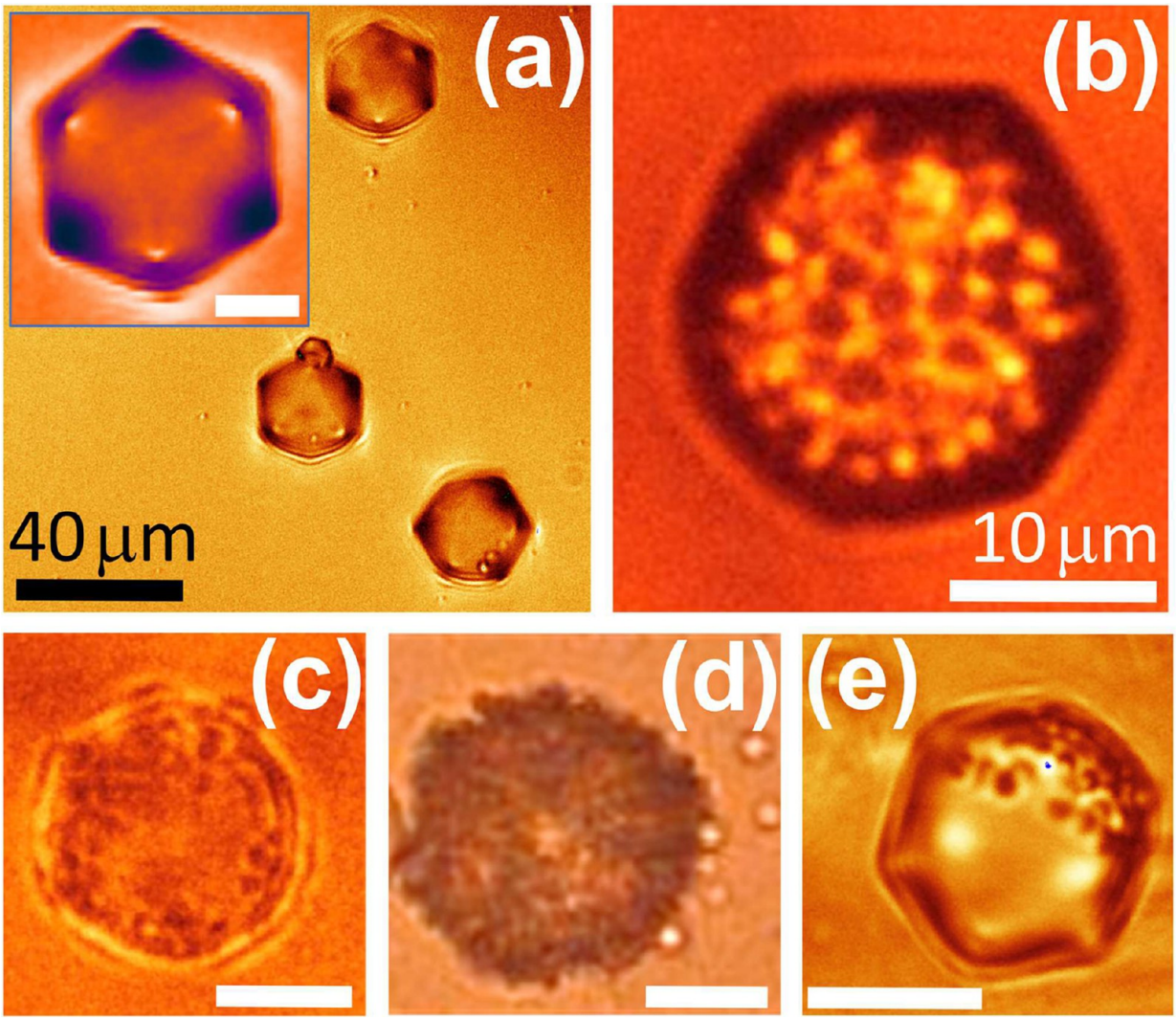

Figure 1. (a) Particle-free droplets, temperature-controllably adopting an icosahedral shape. Note that the bulk of the droplet remains liquid. Similar shapes are obtained with either SHS (main panel) or C_{18}TAB (inset) employed for droplets' stabilization. Remarkably, the icosahedral symmetry survives for droplets densely covered by (b) hydrophobic PMMA, (c) hydrophobic silica, and (d, e) hydrophilic polystyrene particles. The same particle-covered shapes were obtained with either SHS (b, d) or C_{18}TAB (c, e) employed. Note that even a highly nonuniform particle coverage, such as in (e), does not disrupt the sphere-to-icosahedron transition. The images were obtained by bright-field light microscopy. All white-color scale bars are 10 μm.

tion on droplet shape transformations, however, remains unexplored. Previous studies, focusing at the behavior of individual colloidal and nanoparticles adsorbed onto the surfaces of interfacially frozen emulsion droplets, demonstrate that upon the droplets' shape transformation into polyhedra, the particles self-position at the vertices of the droplets,[16,19,25,26] yet the potential effects of surface-adsorbed particles on droplet shape transformations have not been investigated. These effects could be further amplified when the interfacial particle density is high,[26] as is often the case in particle-surfactant costabilized emulsions. Despite this fact, S−I transformations in such emulsions have never been studied, limiting their potential application in real-word systems that are typically costabilized by both particles and surfactants.

We demonstrate that the S−I droplet shape transformations are robust, even in the presence of surface-adsorbed colloidal particles. Remarkably, the droplets' icosahedral symmetry survives even when the surface particle density approaches the close-packing limit. This behavior is surprising, as the surface-adsorbed colloidal particles pierce through the interfacially frozen crystal, thus disrupting its closed-surface topology. We rationalize our observations by computer simulations, demonstrating that hard interfacial crystal inclusions do not interfere with the icosahedron formation. Remarkably, the strong temperature-dependence of γ in the interfacially frozen regime[2] allows the particle-covered liquid icosahedra to be destabilized by cooling, leading to additional shape transformations, followed by particles' detachment from the interface, self-division of particle-covered droplets, or oil extrusion. The observed phenomena open exciting avenues for the formation of polyhedral colloidal nanocapsules,[27] cargo delivery, release, and other nanotechnology applications.[28] In particular, the significant local enhancement of interfacial stress and the decrease in the radius of curvature at specific surface locations, taking place upon the droplet's shape transformations, enable precise decoration of droplets with surface ligands[3,16] for the formation of liquid or solid[18] superstructures, and facilitate the nanoengineering of interfacial

https://doi.org/10.1021/acsnano.4c13476
ACS Nano XXXX, XXX, XXX−XXX

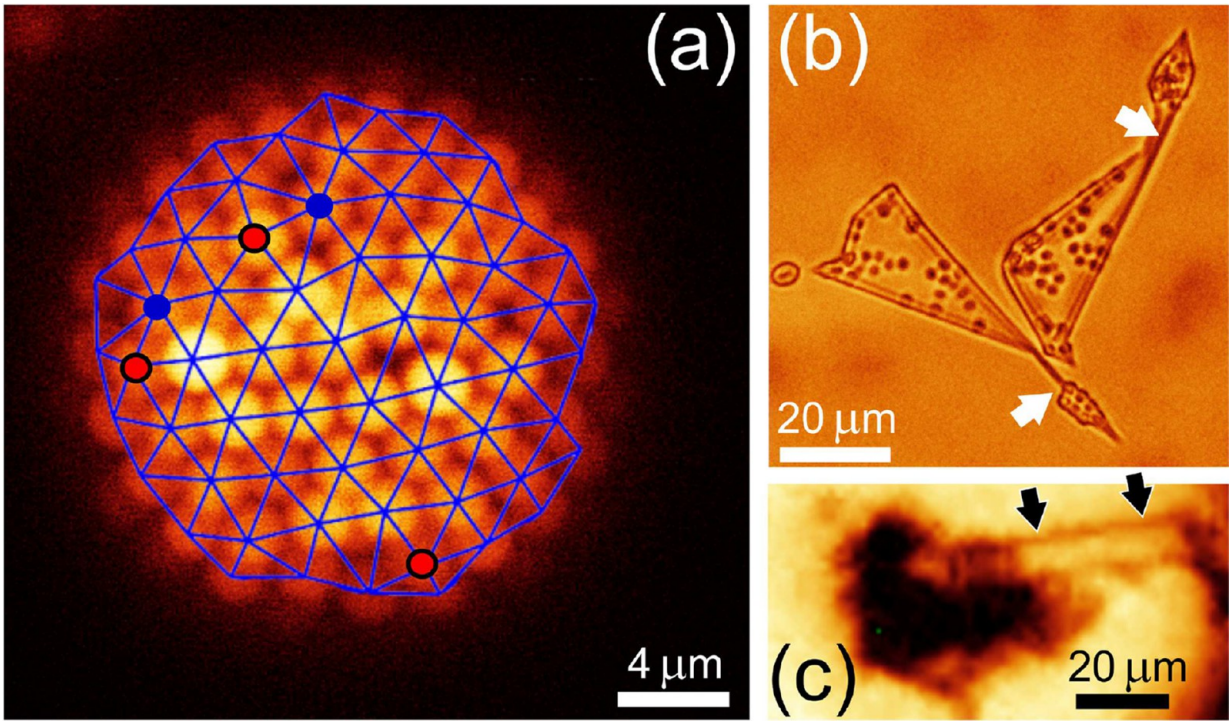

Figure 2. (a) PMMA colloidal particles, covering an emulsion droplet, are almost closely packed. Delaunay triangulation (blue lines) demonstrates that most particles have 6 nearest neighbors. The nonzero Gaussian curvature of droplets' surfaces dictates the formation of structural defects. In particular, a few lattice sites where the coordination number is 5 (marked by black-outlined red dots) or 7 (blue dots), rather than 6, are seen in this confocal microscopy image. (b) Triangular mother droplets extrude (PMMA) particle-covered daughter droplets. For the formation of the daughter droplet, the particles first concentrate near the sharpest vertex of the mother droplet. Next, the vertex region elongates, so that a neck is formed between this region and the mother droplet (see the white arrow in the top-right corner of the image). Further thinning of the neck allows the separation of the daughter droplet from the mother droplet, so that only a thin tube connects between the two (white arrow at the bottom). (c) Formation of a thick oil protrusion (marked by black arrows), emanating from a mother droplet densely covered by the Janus polystyrene particles.

fracture lines. The remarkable variation in total interfacial area allows for fine-tuned molecular exchange between oil and water phases with minimal temperature changes, which holds potential for applications in diverse fields such as chemical engineering and pharmaceutics. The underlying mechanisms may also play a critical role in biological systems, including "lipoproteins", human plasma lipid droplets stabilized by amphiphilic phospholipid monolayers and decorated with colloid-like protein inclusions.[16,29]

RESULTS AND DISCUSSION

As a baseline for our studies of particle-covered emulsion droplets, we first demonstrate the fascinating liquid icosahedral shape obtained in the particle-free system: a hexadecane [$CH_3(CH_2)_{14}CH_3$, denoted as C_{16}] droplet, stabilized in water by ∼1 mM concentration of an anionic sodium hexadecyl sulfate surfactant [$CH_3(CH_2)_{17}SO_3Na$, denoted as SHS] (Figure 1a). Similar shapes are obtained for many other alkane:surfactant combinations[3,16,30] and particularly with the cationic octadecyltrimethylammonium bromide surfactant [$CH_3(CH_2)_{17}N(Br)(CH_3)_3$, denoted as C_{18}TAB], being used for droplets' stabilization (1 mM), instead of the SHS [inset to Figure 1a]. For droplets of these dimensions, thermal motion is dominated by buoyancy. Therefore, one of the icosahedron's facets aligns in parallel with the top wall of the sample-containing capillary, so that the droplet's perimeter appears as a hexagon in a bright-field image. While the 6 vertices of this hexagon are not precisely at the same height, this difference is below the axial resolution of bright-field microscopy,[31] so that the icosahedral droplets are readily distinguished by the hexagonal appearance of their perimeter. The three vertices of the top horizontal facet, above the focal plane, appear as bright dots, while the ones on the bottom facet appear dark and slightly misplaced toward the adjacent vertices of the hexagonal perimeter. This apparent distortion is an optical artifact due to the light refraction at the droplet's interfaces, as evident by the confocal cross sections of the particle-free droplets, manifesting an almost perfect icosahedral symmetry.[2]

When a small number (≤12) of particles is adsorbed to the surface of an icosahedral droplet, the particles do not disrupt the icosahedral shape of the droplet and spontaneously self-position at its vertices.[16,19,25,26] Remarkably, since a surface-adsorbed particle pierces through the interfacially frozen crystal covering the droplet, the crystal's topology changes upon the particle's adsorption, from a closed-surface to an open surface. An open surface is topologically equivalent to a plane, so that according to the topological Euler's polyhedron formula, no structural defects are necessary for this surface to be covered by an hexagonal lattice.[7] However, the high Gaussian curvature of such a lattice leads to significant in-plane deformations, which may be partially relieved by the formation of disclinations.[15] In particular, when a single colloidal particle is adsorbed to the droplet's surface, the interfacial crystal would reduce its elastic energy by the formation of 12 disclinations maximally separated on the spherical surface, with one of these disclinations coinciding with the surface-adsorbed

https://doi.org/10.1021/acsnano.4c13476
ACS Nano XXXX, XXX, XXX−XXX

particle's position.[16,32,33] These disclinations, dictated by the elastic energy, rather than the crystal's topology, drive the S−I transformation, precisely as the topology-dictated ones. Consequently, as long as the number of surface-adsorbed particles is ≤12, these particles are self-positioned at the disclinations, emerging, upon the S−I transformation, at the vertices of the liquid icosahedron.[16,19,25] However, when the number of surface-adsorbed particles exceeds the 12 vertices of the icosahedron, some particles reside at defect-free positions, so that the icosahedral shape of the droplet is expected to undergo a significant distortion.

To test for the possible impact of a large interfacial particle concentration on the droplets' self-faceting transformations, we suspend hydrophobic PMMA (poly(methyl methacrylate)) colloidal particles[34] of radius $r \approx 1.2$ μm, in the dispersed C_{16} oil phase, stabilized by SHS. These PMMA particles are sterically stabilized by PHSA (polyhydroxystearic acid) and fluorescently labeled for confocal microscopy. The particles coadsorb, together with the SHS surfactant, to the droplets' interfaces. We estimate their interfacial contact angle as 152.3 ± 1.4° [see Supporting Information (SI)]. At a high temperature (T = 30 °C), the droplets are spherical (see SI, Movie S1). Upon cooling to $T \lesssim 25$ °C, the droplets undergo a self-faceting transition, with the hexagonal perimeter of the self-faceted droplets allowing their identification as icosahedra (Figure 1b; SI Movie S2). The formation of an icosahedral shape by droplets with their surfaces densely packed by the colloids is quite surprising, as the interfacial crystal is pierced by >150 colloidal particles. The corresponding >150 holes in the interfacial crystal were expected to significantly perturb its elastic stress map, leading to spatial redistribution of the 12 vertex-inducing disclinations and to the formation of multiple additional 5- and 7- fold disclinations.

To investigate the mechanism allowing the S−I transition to take place in particle-covered droplets, we resolve the individual surface-adsorbed colloidal particles, employing laser-scanning fluorescent confocal microscopy. We observe that the particles form an almost close-packed lattice, with only a few particle-size voids and defects visible. These defects, clearly resolved by Delaunay triangulation (Figure 2a), stem from the finite Gaussian curvature of droplets' surfaces. Notably, while only 12 5-coordinated defective lattice sites are dictated by topological considerations,[16] additional pairs of 5- and 7- coordinated lattice sites are clearly visible in Figure 2a, in agreement with previous experiments and theoretical models of Gaussian curvature-induced geometrical frustration of the hexagonal order.[10,35] In particle-free self-faceting droplets, a similar geometrical frustration of the *molecular* crystal, induces sufficient extensional stress for the lattice to buckle out of the plane, overcoming the interfacial tension and leading to the S−I transition.[15] Colloidal crystals covering the surfaces of spherical liquid droplets have been previously demonstrated to exhibit frustration-induced disclinations.[9] However, these systems do not exhibit (molecular) interfacial freezing, and the high interfacial tension does not allow the stress of the colloidal crystal to induce a faceting transition of the droplets.[9] In our system, the interfacial freezing results into a dramatic reduction of $\gamma(T)$ on cooling,[6,36] so that the surface energy penalty for droplet's shape transformation may be much smaller.

To explore the possibility that the S−I transition is driven by the elastic stress of the geometrically frustrated colloidal crystal, we form an ultralow-γ heptane emulsion, stabilized by AOT (dioctyl sulfosuccinate sodium salt, 1 mM) in a 40 mM aqueous NaCl solution.[37] By temperature control of this emulsion, we vary the oil−water γ value from ≈0.1 mN/m to ultralow <1 μN/m. As above, we suspend PMMA colloidal particles in the oil phase, so that they adsorb to the interface, forming a densely packed interfacial packing. We employ a complete three-dimensional confocal tomography,[31] confirming that the colloidal packing fully covers the surfaces of our droplets (see SI, Movies 3 and 4). Yet, in spite of the complete and dense interfacial colloidal packing, no faceting of the droplets is observed, even for the lowest γ. Only the smallest droplets, where the particles adsorbed at the opposite sides of the droplet are in contact, exhibit faceted shapes. However, these shapes are controlled by the particles' packing constraints inside the droplets, a mechanism unrelated to our present studies.[38] To rationalize the absence of self-faceting for the large, surface-controlled, droplets, we note that the Young's modulus of a colloidal crystal[39−41] is, by dimensional analysis, of the order of $k_BT/r^2 \approx 3 \times 10^{-9}$ N/m. For the extensional stress of such crystals to dominate the droplets' shapes, γ must be $\lesssim 10^{-9}$ N/m, which is 3 orders of magnitude lower than practically achievable in the present, or any other previously studied, stable and controllable, molecular system. In particular, while in our emulsions γ vanishes at T_{SE}, as described below, $\gamma(T)$ dependence[2,16,42] is far too strong to controllably keep γ between 0 and 10^{-6} N/m. Finally, while interface-mediated particle interactions were previously demonstrated to enable the formation of high Young's modulus colloidal crystals,[43] these interactions vanish at low γ, not allowing the droplet faceting regime to be reached by this route. Thus, the present observation of faceting in particle-covered droplets cannot be driven by the colloidal crystal and it must be attributed to the molecular interfacially frozen crystal.

As the stabilizing surface layer of the PMMA particles exposes PHSA alkyl tails of the same length as the C_{16} alkane and the SHS surfactant, the solid−liquid interface of these particles may undergo a freezing transition,[44] forming a mixed PHSA:C_{16} (or PHSA:C_{16}:SHS) two-dimensional crystal. If the structure of this hypothetical PHSA crystal is sufficiently similar to the structure of the C_{16}:SHS crystal forming at the liquid−liquid interface, the PHSA crystal may cover the holes pierced by the particles in the C_{16}:SHS crystal. A single coherent crystalline structure thus covering both the particle surfaces and the interparticle interstices, would revalidate the Euler's polyhedron formula and the consequent self-faceting mechanism. To test this scenario, we repeat our experiments using hydrophobic trimethylsilyl-covered silica particles (r = 0.75 μm; contact angle ≈130.6 ± 3.2°). The small trimethylsilyl group at these particles' surfaces has no alkyl tails and does not promote the formation of a mixed interfacial crystal with the C_{16} alkane.[45] Surprisingly, the silica colloids-covered droplets exhibit a S−I transition precisely as the ones covered by the PMMA particles (Figure 1c). Thus, the hypothetical interfacial crystallization of PHSA is unable to explain the mechanism behind the observed shape transformation.

To test the generality of the observed S−I transition, we repeat the experiments using various sizes of PMMA and silica particles. These particles have the same surface chemistry as above, but their radii range from 50 nm to 2.5 μm, so that their volumes span more than 5 orders of magnitude. Notably, some of these particle batches are highly monodisperse (∼2%), while

https://doi.org/10.1021/acsnano.4c13476
ACS Nano XXXX, XXX, XXX−XXX

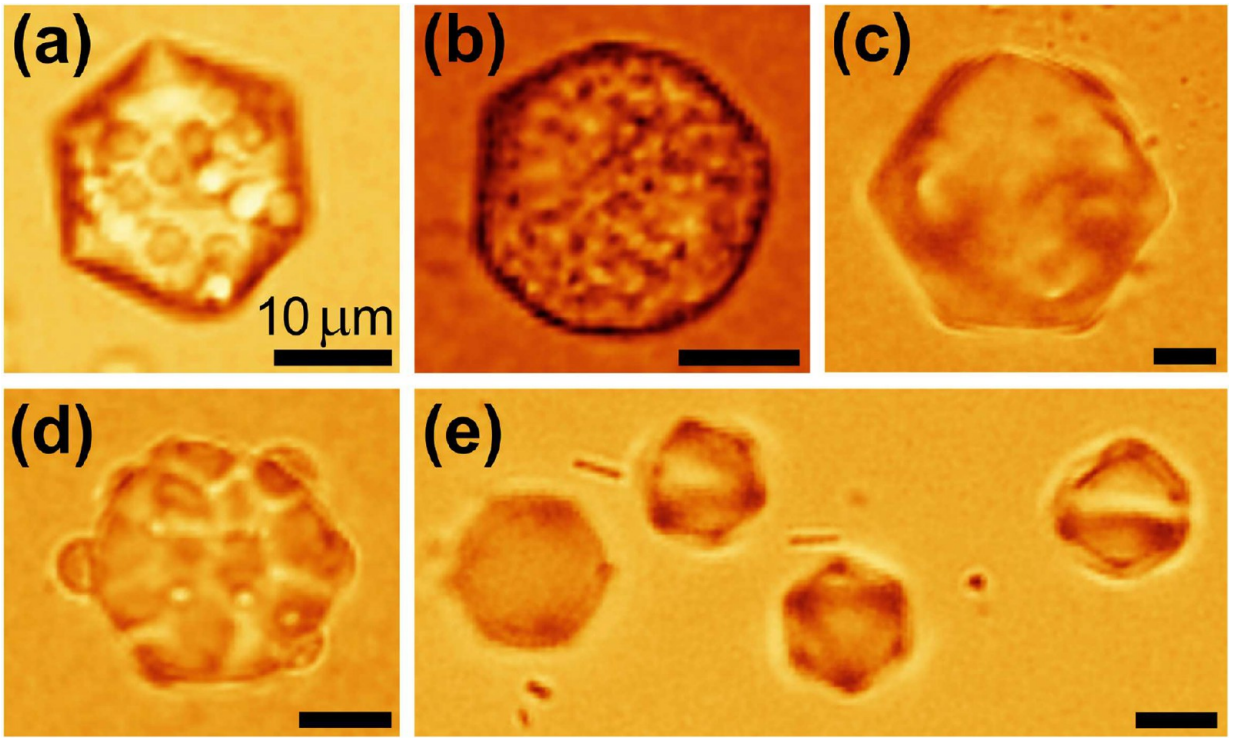

Figure 3. Sphere-to-icosahedron transition of oil-in-water droplets persists for droplets covered with particles of different types and sizes. PHSA-stabilized PMMA particles of radii: (a) $r = 1.75\ \mu$m; (b) $r = 400$ nm. Trimethylsilyl-covered silica particles: (c) $r = 250$ nm; (d) $r = 2.5\ \mu$m; (e) $r = 50$ nm. All scale bars are 10 μm.

the others have a wider size distribution. Yet, in all of these samples, we observe a similar S−I shape transformation of the droplets, strongly emphasizing the general nature of this effect (see Figure 3).

To confirm that the particles truly pierce through the droplets' surfaces, excluding the formation of a nonwetting surface-adjacent packing of colloids,[46,47] we repeat the experiment with particles exhibiting a vastly different interfacial wettability: hydrophilic polystyrene colloids ($r \approx 0.35\ \mu$m). The contact angle of these particles is $67.8 \pm 1.4°$ (see SI), so that they adsorb to the interface from the aqueous continuum. Remarkably, droplets densely packed with the *hydrophilic* particles exhibit similar shape transformations to the ones observed with the *hydrophobic* particles [cf. Figure 1d−e and Figure 1b−c; see also Figure S2 in SI], indicating that interfacial wettability does not play a significant role in this phenomenon and confirming that piercing of the interface by multiple particles does not eliminate the S−I transformation.

To elucidate the mechanism of the observed shape transformations, we carry out computer simulations of particle-decorated droplets, employing the PyMembrane framework.[48] The interfacially frozen crystal is modeled by a Hookean springs triangulation lattice on a unit sphere ($R = 1$), including $N = 2562$ lattice sites. A similar methodology has been employed in a wide range of previous studies of interfacial crystals and membranes.[2,3,8,11,13,15,19,49,50] The initial configuration of this lattice has the minimal number of defects allowed by the Euler's formula: 12 5-fold disclinations, maximally separated on the sphere. The extensional energy of the lattice is[2,3,13] $E_s = (k/2)\sum_{\langle ij\rangle}(|\mathbf{r}_i - \mathbf{r}_j| - a)^2$, where k is the Hooke's constant, $a \approx 0.075R$ is the average edge length, and the summation is carried out over all nearest-neighbor lattice sites. Setting $a = (4\pi R^2/N)^{1/2}$ does not qualitatively change the results. The bending energy is[2,13] $E_d = (\kappa/2)\sum_{\langle IJ\rangle}(\hat{\mathbf{n}}_I - \hat{\mathbf{n}}_J)^2$, where κ is a constant proportional to the bending modulus,[13] and the summation is over all nearest-neighbor plaquettes of the triangulated surface, with unit normals $\hat{\mathbf{n}}_I$. The dimensionless ratio kR^2/κ is set to 8×10^4, so that the Föppl-von Kármán (FvK) number[2,13] $\approx 10^5$ is well above the minimal condition for the buckling S−I transformation.[13] This choice is motivated by the FvK number of the experimental particle-free droplets, which is very high.[2,15]

To decorate the simulated droplet by particles piercing holes of radius $r = 0.1R$ and total area fraction η in the interfacial crystal, we position the centers of $N_c = 4\eta/r^2$ particle-pierced holes at random lattice sites, employing the random sequential adsorption algorithm.[51] When both ends of a Hookean spring are located inside a particle-pierced hole, the spring is replaced by an unstretchable solid constraint, so that its two ends move together as parts of a solid particle. When one end of a spring is inside a hole and the other - outside, the spring's Hooke's constant is set to $k/2$. As no thermal shape fluctuations or particle displacements are visible in our experiments, we are only interested in the lowest-energy configuration of the system. We relax the energy E of the Hookean lattice by classical Monte Carlo (MC) dynamics, involving three-dimensional displacements of lattice sites and particle centers by $\Delta r \approx 10^{-3}R$. In addition, we also allow bond flips, where an edge (i.e., a spring) shared by two triangles of the lattice is removed and the two lattice sites opposite to it are reattached by a new edge (i.e., a new spring), as demonstrated in the inset of Figure 4c.[48] Edge flips are only allowed for particle-free lattice sites. Even though the bond flip attempts are undertaken at the same rate as the lattice site displacements, the rate of the accepted bond flips is very low. To increase the rate of edge flips, we use a higher temperature, T_e, for the edge flips and a

https://doi.org/10.1021/acsnano.4c13476
ACS Nano XXXX, XXX, XXX−XXX

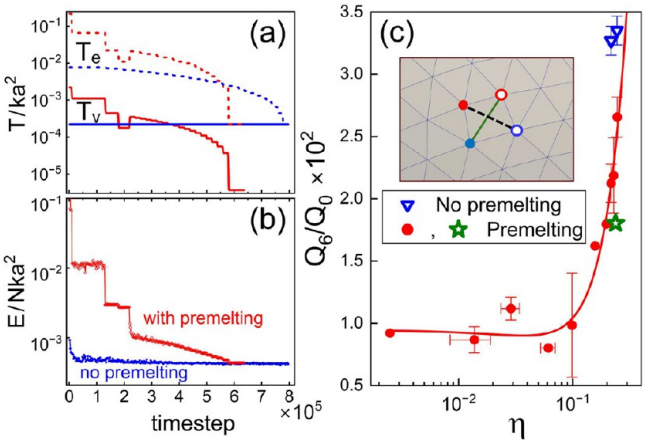

Figure 4. Computer simulations reproduce the experimental observation that the surface-adsorbed particles do not disrupt the droplets' S−I shape transformation. (a) Monte Carlo annealing temperatures used for edge flipping (T_e, dashes) and lattice site displacements (T_v, solid lines), in simulations with (red) and without (blue) the premelting of the lattice. The corresponding energy relaxation plots, for holes' volume fraction $\eta \approx 0.25$, are shown in (b). Note that the final energies reached by both procedures are almost identical, strongly supporting our conclusions. (c) The extent of the icosahedral symmetry, measured for the simulated droplets by a rotation-invariant combination of spherical harmonics' decomposition coefficients Q_6/Q_0, increases as a function of the particle-pierced holes' volume fraction η. The result of a much longer simulation run is marked by a green star. Standard errors are shown where multiple data points were binned. The solid line is guide to the eye. Note the very good agreement between data obtained with (red, green) and without (blue) lattice premelting. Inset: An edge-flipping procedure is employed in our simulations, to enable lattice defect formation and migration. Here, this procedure replaces the solid green bond by the dashed black one, allowing a pair of 5- (red) and 7- (blue) coordinated lattice sites, to migrate to new positions, marked by white-filled red and blue circles, respectively.

lower T_v for all other degrees of freedom. This choice is fully adequate, as our simulations only aim at the lowest energy configuration.

With the annealing procedure of Figure 4a (blue lines), the energy decreases and eventually saturates (Figure 4b, blue). Remarkably, the resulting shape of the particle-decorated droplet has a clear icosahedral symmetry, as demonstrated in Figure 5a, in full agreement with the experimental images. To test the robustness of this energy minimum, we repeat the simulations starting from higher T_e and T_v. With this choice of the initial temperatures, the simulated interfacial crystal melts prior to the annealing procedure (red lines in Figure 4a). Yet, the long-time saturation E values almost coincide for both of the annealing procedures (cf. red and blue in Figure 4b). Note also the good agreement between the corresponding icosahedral droplet shapes (Figure 5), strongly suggesting that this configuration corresponds to a global E minimum.

For a more quantitative characterization of droplets' shapes, we employ the spherical harmonics decomposition[13] of lattice site positions. With the origin located at the center of the droplet and the polar coordinates of a lattice site denoted as (R_i, θ_i, ϕ_i), we obtain the spherical harmonic coefficients: $Q_{lm} = \sum_j R_j Y^*_{lm}(\theta_j, \phi_j)$, where the summation is over all lattice sites (including the ones inside the particle-pierced holes), and Y_{lm} are the spherical harmonics. The rotation-invariant Q_{lm} combinations, $Q_l = 4\pi(2l+1)^{-1} \sum_{m=-l}^{l} |Q_{lm}|^2$, quantify the symmetry of the simulated surface.[13] For icosahedrally symmetric shapes, the first nonvanishing harmonic is $l = 6$. Thus, we quantify the extent to which the icosahedral symmetry is present by Q_6/Q_0. Strikingly, while a very weak decrease in Q_6/Q_0 seems to take place at low η, this quantity exhibits a dramatic *increase* at $\eta > 0.1$ (red symbols in Figure 4c). This counterintuitive trend, observed in simulations where surface crystals were allowed to melt prior to their cooling to the self-faceting transition, is further corroborated by Q_6/Q_0 values obtained without the crystals' premelting (blue triangles in Figure 4c). Accordingly, the results obtained with extra-long simulations (1.8×10^7 time steps; a green star symbol) agree with our typical simulations (6.38×10^4 steps; 2−3 replicates per point), further supporting the observed trend.

To rationalize the experimentally observed persistence of S−I transitions at high concentrations of surface-piercing particles, as well as the simulated increase in the icosahedral symmetry metric Q_6/Q_0 with η, it is important to note that the incorporation of particles into the interfacial crystal increases the local stiffness of this crystal. While a particle-free lattice has a *finite* extensional modulus, the modulus of the simulated particle-pierced holes is effectively infinite. Since the S−I transition is driven by the in-plane extensional deformation of the spherical hexagonal crystal,[16,32,33] the tendency to undergo the transition increases with the Young's modulus,[2,13,14,16] Y_{2D}. Accordingly, the "holes" in the simulated crystalline shells and the colloidal particles at the surface of the experimental droplets play a role of high-rigidity inclusions and do not disrupt the S−I transition. Importantly, these multisite inclusions are unable to form a segregated phase, so that our droplets are fundamentally different from the multicomponent vesicles.[49,50] Simulations have shown, that in such vesicles, the component having a higher Y_{2D} is repelled from the high-strain regions, as the stress energy (at a given strain) is proportional to Y_{2D}. Thus, it is energetically favorable to have the vertices covered by the low-Y_{2D} component. The colloidal particles exhibit the opposite behavior. Particles pierce through the lattice, eliminating its highest-stress patches. With that, the particles do not undergo stretching, regardless of their on-surface position. Consequently, the particles are attracted by the highest-strain (and stress) regions of the lattice, ending up at the vertices of the self-faceted droplets.[19,25] When the particles' number exceeds the vertices' number of the icosahedron (12), the particles preferentially self-locate onto the faceted droplets' edges, where the curvature is higher (see Figure S3 in the SI). In simulations with low particle numbers, the symmetry may be somewhat disrupted, as the different facets (and edges) are unable to get a similar number of particles. As the particle number increases, the uniformity of their on-surface distribution is improved, leading to the observed increase in Q_6/Q_0. Future experiments, employing high-resolution 3D droplet shape analysis (e.g., by means of 3D electron tomography[52] of UV-polymerized particle-covered droplets[18]), may allow this simulated trend to be verified.

Finally, in addition to the equilibrium phenomena described above, our particle-covered droplets also exhibit fascinating nonequilibrium behavior. In the interfacially frozen regime, $\gamma(T)$ exhibits a high and positive temperature slope.[2,42] Consequently, γ vanishes on cooling to $T = T_{SE}$, which is higher than the bulk freezing temperature of the droplets, yet slightly lower that the temperature of the S−I transi-

https://doi.org/10.1021/acsnano.4c13476
ACS Nano XXXX, XXX, XXX−XXX

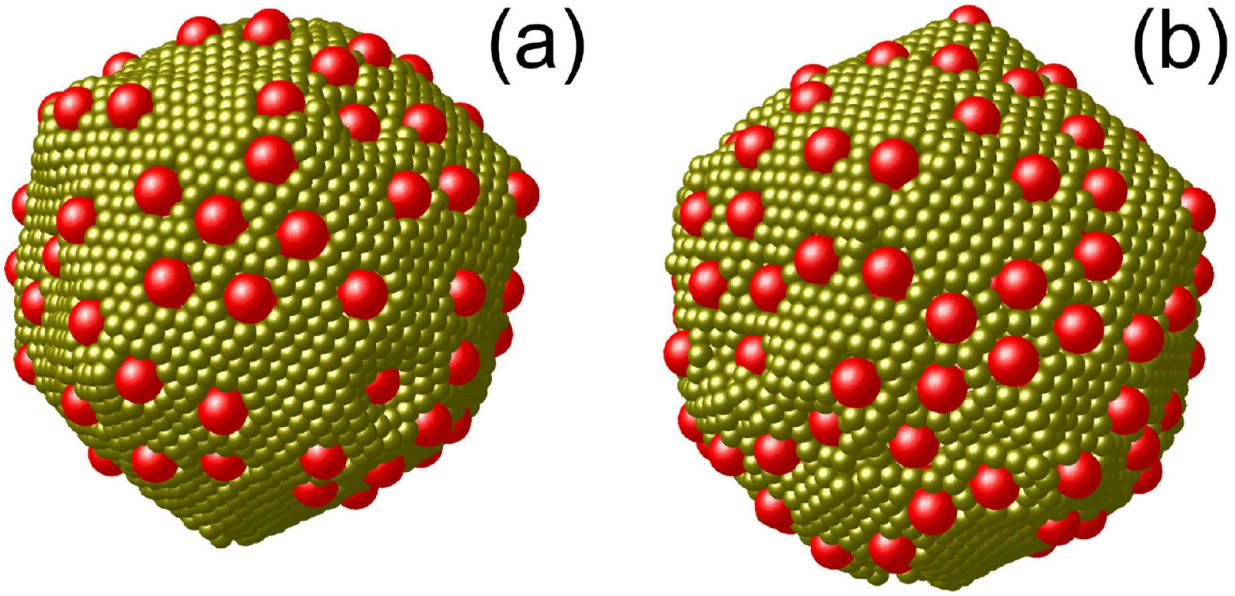

Figure 5. Computer simulations of S−I transitions of particle-covered droplets ($\eta \approx 0.25$). The particles are red, the interfacial crystal's lattice is yellow. The droplets are shown to adopt an icosahedral shape, in spite of the significant concentration of particles at their surfaces. Note the hexagonal perimeter, typical for the icosahedral shapes. The results are robust for vastly different simulation protocols: (a) No premelting of the lattice; (b) After the introduction of the particles, the lattice is premelted, prior to its cooling to the shape transformation temperature.

tion.[2,14,16,53] Furthermore, on cooling to $T < T_{SE}$, γ transiently becomes negative, so that the area of the droplets' crystalline interfaces spontaneously starts growing.[54] In this regime, the *particle-free* icosahedral droplets distort into higher surface-area shapes,[15] such as interfacially frozen cylindrical tubules,[54] hexagonal and tail-bearing triangular platelets,[2,16] and more. When *particle-covered* droplets are cooled to $T < T_{SE}$ and distort into higher-area shapes, we observe several different routes for the growth of their interfacial area. The simplest route is the desorption of surface-adsorbed particles, upon which the interfacially frozen crystal grows at the expense of the vanishing particle-pierced hole. We observe this route for both the hydrophobic silica and the hydrophilic polystyrene particles, but not for the PHSA-stabilized hydrophobic PMMA. Temperature-triggered desorption of surface-adsorbed colloids, which has never been achieved for the conventional Pickering emulsions, is promising for delivery and release applications. An alternative route for interfacial area growth is the self-division of the droplet, achieved by formation of an elongating particle-free neck, separating one part of the particle-loaded droplet from the other. The neck thins and elongates, eventually disappearing beyond the resolution limit of the light microscopy (Figure 2b, SI Movie S5). This route was observed for the PHSA-stabilized PMMA colloids. The third route is the formation of a tail-like cylindrical protrusion, penetrating through the particle-covered interface (Figure 2c). We have hitherto observed this route only for droplets covered by the Janus particles, μm-scale amphiphiles, one surface hemisphere of which is hydrophobic and the other - hydrophilic.[55] While the growth of multiple thin "Gorgon hairs" has been reported for droplets covered by jammed hydroxyl latex particles, the authors attributed this phenomenon to a different physical mechanism.[26]

To test the generality of these routes, we have undertaken experiments with PHSA-stabilized PMMA particles of radii $0.4 < r < 1.74$ μm and trimethylsilyl-covered silica particles of radii $0.05 < r < 2.5$ μm. In all of these systems, the PMMA-covered droplets exhibited self-division by the neck formation (see SI Figure S4), whereas silica particles exhibited simple desorption. Interestingly, the observation that both *hydrophobic* silica and *hydrophilic* polystyrene particles follow the same route, despite the significant difference in their interfacial contact angles, indicates that the different routes are influenced by some other parameter. We hypothesize, as above, that the sterically stabilizing PHSA layers of the PMMA particles cocrystallize[44] with the interfacially frozen alkane and surfactant. Such a cocrystallization would dramatically reduce the energetic drive for particles' expulsion from the interface. Silica and polystyrene particles, which have long alkyl tail-bearing stabilizing layers at their surfaces, do not participate in interfacial freezing and therefore undergo simple desorption. Finally, the lack of desorption of Janus particles at $T < T_{SE}$ is due to the inability of either bulk phase to wet both hemispheres of the particle. Therefore, these particles do not leave an oil−water interface at $\gamma = 0$, contrasting with all other particle types. In addition, the Janus particles exhibit a somewhat reduced stability, with some clustering of these particles apparently taking place at the interface. As a result, the droplet increases its interfacial area by protrusion formation. The present brief description of the rich variety of nonequilibrium phenomena observed in interfacially frozen Pickering emulsions demonstrates that these systems deserve further systematic studies, currently underway, and potentially enable hitherto unexplored methods in nanotechnology and beyond: internally or externally triggered destabilization of Pickering emulsions for cargo release in pharmaceutical and other nanotechnology applications, triggering of self-propulsion[56] in particle-covered emulsions, synthesis of active matter with anomalous physical properties,[53,57] energy-efficient formation[58] of Pickering emulsion droplets at the nanoscale,[14] and more.

https://doi.org/10.1021/acsnano.4c13476
ACS Nano XXXX, XXX, XXX−XXX

CONCLUSIONS

We have demonstrated, that interfacially frozen Pickering emulsions, costabilized by molecular surfactants, exhibit temperature-controlled sphere-to-icosahedron transitions. We reproduced the experimental observations by computer simulations, elucidating the physical mechanism driving the transitions. In particular, even though the surface-adsorbed colloidal particles disrupt the topology of the interfacially frozen molecular crystal, the geometrical frustration of the crystal's hexagonal order in the presence of the Gaussian curvature induces an in-plane stress inside the crystal. Since the particle-pierced holes in the interfacial crystal are effectively incompressible, these holes are unable to relieve the stress. Consequently, when the interfacial tension is sufficiently low, the stress is relieved by the sphere-to-icosahedron out-of-plane buckling transition. On cooling to $T < T_{SE}$, the icosahedra distort and further increase their surface area by either particles' desorption, neck-mediated division, or tail formation. The observed phenomena open avenues in manipulation of emulsion droplets. Particularly promising may be the implementation in this system of particles responding to external, e.g., magnetic or light, fields. The formation of similar Pickering emulsions with surface-adsorbed active self-propelling particles may allow the surface-mediated interactions between the particles and the topological defects to be explored, revealing exciting physical phenomena and expanding the fundamental toolbox of nanotechnology, en route to nanoengineering of smart active matter.

SUPPORTING MATERIALS AND METHODS

Materials. The hexadecane (TCI, >98% pure), was percolated 2−3 times through a freshly activated basic alumina powder column to remove acidic polar impurities. The cationic octadecyltrimethylamonium bromide (C_{18}TAB, Sigma-Aldrich, 98% pure) surfactant was recrystallized twice from a methanol−acetone solution, then twice recrystallized from a hexane−acetone solution. The anionic sodium hexadecyl sulfate surfactant (SHS, Acros Organics, 98+%) was used as received. Millipore Ultrapure 18.2 MΩ·cm water was used throughout.

Hydrophobic Colloids. The hydrophobic fluorescent PMMA colloids were synthesized according to the classical protocol,[34] then transferred to hexadecane and washed several times by decantation. The hydrophobic fluorescent trimethylsilyl-covered silica colloids (Sicastar redF) were obtained from Micromod, suspended in hexadecane and washed by decantation.

Hydrophilic Colloids. Hydrophilic polystyrene particles are synthesized by dispersion polymerization. 0.03 g of poly(vinyl pyrrolidone) (Mw ≈ 55,000) is dissolved in 75 mL of isopropyl alcohol (99.9%), in a 250 mL flask. 0.02 g of ammonium persulfate (98%) dissolved in 9 mL of DI water is then added to the flask as the initiator. Styrene (≥99%) is percolated through a column of inhibitor remover (for removing tert-butylcatechol, Sigma Aldrich) once, and 6.6 mL of it is added to the flask. The flask is sealed by a rubber stopper, mounted onto a tumbler (IKA RW 20 digital), and tumbled at 100 rpm for 24 h in an oil bath at 70 °C for polymerization. After polymerization, the particles are washed four times with DI water using centrifugation.

Amphiphilic Janus Colloids. Janus particles are synthesized by seeded emulsion polymerization followed by hydrolysis. To use polystyrene particles as seed particles, we prepared a 20 wt % polystyrene particle dispersion by dispersing the particles in 1 wt % poly(vinyl alcohol) (PVA, Mw = 13,000−23,000, 87−89% hydrolyzed) aqueous solution. A 20 wt % monomer emulsion is prepared by homogenizing (IKA Ultra-Turrax T25 basic) a mixture consisting of styrene, tert-butyl acrylate (tBA, Sigma-Aldrich, 98%), 1 vol % divinylbenzene (DVB, Sigma-Aldrich, 55%), and 1 wt % initiator 2,2′-azobis(2,4- dimethylvaleronitrile) (V-65B, Wako) with 1 wt % PVA aqueous solution. The polystyrene particle dispersion is homogenized with the monomer emulsion at 8000 rpm with the volume ratio of the particle dispersion and monomer emulsion being 1:4. The mixture is transferred to a 250 mL flask, which is then mounted on a shaker table. After 12 h of mixing at 200 rpm, seeded emulsion polymerization is performed by tumbling the particle−monomer mixture in an oil bath at 70 °C at 200 rpm for 6 h. The particles are washed with DI water at least six times by centrifugation, after polymerization. To hydrolyze tBA, the particles are mixed with an acid mixture consisting of 80 vol % trifluoroacetic acid (99%) and 20 vol % formic acid (≥95%) at 200 rpm with a shaker table, for 24 h. The volume ratio of particles and acid mixture is 1:40. The hydrolyzed particles are washed with DI water 6 times by centrifugation. This protocol has previously been demonstrated[59] to yield Janus particles with a contact angle of ≈90°.

Preparation of Surfactant Costabilized Pickering Emulsions. To form an emulsion stabilized by hydrophobic particles, we first suspend the particles at a high density (∼10−20% v/v) in hexadecane and vortex the suspension for particle density homogenization. Next, the suspension is introduced into a ∼1 mM aqueous surfactant suspension, with the oil comprising ∼1−2% (w/w) of the resulting emulsion. To form the emulsion droplets, the system is mixed by a magnetic stirrer for ∼2 min, at ∼50 °C. Note, while PMMA-covered emulsions were co-stabilized by SHS, the emulsions covered by the Sicastar silica particles were co-stabilized by C_{18}TAB. No self-faceting transitions were observed in emulsions costabilized by Sicastar particles and SHS, probably due to a preferential adsorption of SHS onto the surfaces of the particles, with the SHS bulk concentration consequently depleted.

To form an emulsion stabilized by the hydrophilic polystyrene particles, we suspend the particles in water ∼1−2%. Next, we introduce H_2O, C_{16}, and the aqueous particles' suspension (87%, 7%, and 6% w/w, respectively) into a container and form a surfactant-free Pickering emulsion, applying a homogenizer. The resulting Pickering emulsion is introduced into either an SHS or a C_{18}TAB solution and gently mixed by a magnetic stirrer at T = 40 °C. The final SHS (or C_{18}TAB) concentration is ∼1 mM.

To form an emulsion costabilized by Janus particles, hexadecane is homogenized with 2 wt % Janus particle dispersion in pure water, forming emulsion droplets with interfaces fully covered by the particles. The emulsion is injected into a microfluidic device made by bonding a polydimethylsiloxane (PDMS) slab with microwell features to a glass slide. After a sufficient number of emulsion droplets settle in the microwells, 3 mM sodium octadecyl sulfate [$CH_3(CH_2)_{17}OSO_3Na$, Thermo Scientific, 98%] solution is pumped into the device, with the flow rate maintained at 100 μL/hr.

https://doi.org/10.1021/acsnano.4c13476
ACS Nano XXXX, XXX, XXX−XXX

Optical Microscopy: Sample Preparation and Imaging. For light microscopy experiments, we load an emulsion into a Vitrocom 0.1 × 2 × 50 mm capillary by capillary action. The loading of the capillaries is carried out while keeping the bulk materials at $T \geq 40$ °C, well above the interfacial freezing transition. Once filled with the sample, the capillary was glued by epoxy with its wide face down onto a brass slide, having a narrow machined opening for optical observations. The slide is inserted horizontally into a homemade temperature-controlled cell, mounted on the translation stage of an inverted microscope. The sample cell employs a pair of Peltier elements for baseplate cooling, thin-film resistive heaters for PID temperature control by Lake Shore model 330, and a 100 kW precision thermistor. This setup was employed in our previous studies of emulsions and is described in the literature.[2,3,14,25,42,60−62]

For confocal microscopy, we employ a Nikon A1R resonant laser-scanning confocal setup, integrated with a Nikon Ti-E bright-field microscope and equipped by the 514 nm and 488 nm diode laser excitation lines. A Nikon DS-Fi1 CCD camera, installed in this setup, was employed for bright-field video acquisition. The confocal and the bright-field imaging serve in our studies as complementary methods, as the fluorescent colloidal particles are almost invisible by the bright-field microscopy, yet clearly visible in the fluorescent confocal imaging mode. Conversely, the oil droplets' interfaces are invisible by the confocal microscopy, as the liquid phases are nonfluorescent, yet clearly visible by the bright-field microscopy. Our setup allows rapid switching between these two imaging modes, without losing the object of focus. In addition, the confocal mode allows a much higher resolution to be achieved, both along the optical axis and in the focal plane, approaching the classical resolution limit of light microscopy. The confocal scanning was carried out in the galvanometric mode, to improve the signal-to-noise ratio of the images. Both the confocal and the bright-field imaging employed dry Plan Apo 20× (NA = 0.75), Plan Fluor 100× (NA = 0.9), and an Extra-Long Working Distance (ELWD) Plan Fluor 60× (NA = 0.7) objectives. These objectives do not physically contact the sample-containing capillary, thus minimizing temperature gradients within the sample.

For bright-field imaging and temperature control of droplets contained in the microfluidic wells (Figure 2c), the microfluidic device is positioned on top of the temperature-control element of the Linkam THMS350V stage, regulating the temperature with a 0.1 °C resolution. To reach the temperature where shape transformations take place, we cool the emulsion at a constant rate, 1 °C/min. Once $T = 19.1° \approx$ TSE −3 °C is reached, the cooling scan is stopped and the emulsion is followed as a function of time. For bright-field microscopy imaging of these emulsions, we employed the iScope IS1053-PLPORi setup by Euromex.

Simulation Codes Availability. The employed simulation codes are available on GitHub.[48] To clone the code, use: git clone --single-branch --branch develop (https://github.com/fdmatoz/pymembrane.git). To install the code, use: python setup.py install The command file for a typical simulation (in Python) is under docs/examples, together with the corresponding output.

ASSOCIATED CONTENT

Supporting Information

The Supporting Information is available free of charge at https://pubs.acs.org/doi/10.1021/acsnano.4c13476.

Supporting Text and Figures: 1. Contact angle measurements; 2. Supplementary Figures; 3. Movie Captions (PDF)

Movie S1: Confocal cross-section height scan ("z-stack") through a spherical surfactant costabilized Pickering emulsion droplet (AVI)

Movie S2: Temperature-controlled sphere-to-icosahedron transition exhibited by a particle-covered oil-in-water emulsion droplet (AVI)

Movie S3: Confocal tomography stack of optical slices through a heptane-in-water emulsion droplet, costabilized by AOT and a dense layer of PMMA particles (AVI)

Movie S4: Confocal 3D reconstruction of heptane-in-water emulsion droplets, costabilized by AOT and PMMA particles (AVI)

Movie S5: Neck formation events, leading to self-division of surfactant costabilized Pickering emulsion droplets (with PMMA particles) (AVI)

AUTHOR INFORMATION

Corresponding Authors

Daeyeon Lee − *Department of Chemical and Biomolecular Engineering, University of Pennsylvania, Philadelphia, Pennsylvania 19104, United States;* orcid.org/0000-0001-6679-290X; Email: daeyeon@seas.upenn.edu

Eli Sloutskin − *Physics Department and Institute of Nanotechnology & Advanced Materials, Bar-Ilan University, Ramat Gan 529002, Israel;* orcid.org/0000-0002-7109-6893; Email: eli.sloutskin@biu.ac.il

Authors

Alexander V. Butenko − *Physics Department and Institute of Nanotechnology & Advanced Materials, Bar-Ilan University, Ramat Gan 529002, Israel*

Emery Hsu − *Department of Chemical and Biomolecular Engineering, University of Pennsylvania, Philadelphia, Pennsylvania 19104, United States*

Daniel A. Matoz-Fernandez − *Department of Theoretical Physics, Complutense University of Madrid, 28040 Madrid, Spain*

Lee Shool − *Physics Department and Institute of Nanotechnology & Advanced Materials, Bar-Ilan University, Ramat Gan 529002, Israel*

Andrew B. Schofield − *The School of Physics and Astronomy, University of Edinburgh, Edinburgh EH9 3FD, U.K.*

Complete contact information is available at: https://pubs.acs.org/10.1021/acsnano.4c13476

Author Contributions

§A.V.B. and E.H. contributed equally to this work.

Notes

The authors declare no competing financial interest.

ACKNOWLEDGMENTS

This research was supported by Grant No. 2110611 from the United States National Science Foundation (NSF) and the United States-Israel Binational Science Foundation (BSF).

D.A.M.-F. thanks the Comunidad de Madrid and the Complutense University of Madrid (Spain) through the Atraccion de Talento program 2022-T1/TIC-24007. The authors thank M. Deutsch for fruitful discussions.

REFERENCES

(1) Berg, J. C. *An Introduction to Interfaces & Colloids: the Bridge to Nanoscience*; World Scientific: Singapore, 2010.
(2) Guttman, S.; Sapir, Z.; Schultz, M.; Butenko, A. V.; Ocko, B. M.; Deutsch, M.; Sloutskin, E. How Faceted Liquid Droplets Grow Tails. *Proc. Natl. Acad. Sci. U.S.A.* **2016**, *113*, 493−496.
(3) Das, S.; Butenko, A. V.; Mastai, Y.; Deutsch, M.; Sloutskin, E. Topology-Driven Surface Patterning of Liquid Spheres. *Nat. Phys.* **2022**, *18*, 1177−1180.
(4) Haas, P. A.; Cholakova, D.; Denkov, N.; Goldstein, R. E.; Smoukov, S. K. Shape-Shifting Polyhedral Droplets. *Phys. Rev. Research* **2019**, *1*, No. 023017.
(5) Denkov, N.; Tcholakova, S.; Lesov, I.; Cholakova, D.; Smoukov, S. K. Self-Shaping of Oil Droplets via the Formation of Intermediate Rotator Phases upon Cooling. *Nature* **2015**, *528*, 392−395.
(6) Sloutskin, E.; Bain, C. D.; Ocko, B. M.; Deutsch, M. Surface Freezing of Chain Molecules at the Liquid-Liquid and Liquid-Air Interfaces. *Faraday Discuss.* **2005**, *129*, 339−352.
(7) Coxeter, H. S. M. *The Beauty of Geometry: Twelve Essays*; Dover Publications: Mineola, NY, USA, 1999.
(8) Kohyama, T.; Gompper, G. Defect Scars on Flexible Surfaces with Crystalline Order. *Phys. Rev. Lett.* **2007**, *98*, No. 198101.
(9) Bausch, A.; Bowick, M.; Cacciuto, A.; Dinsmore, A.; Hsu, M.; Nelson, D.; Nikolaides, M.; Travesset, A.; Weitz, D. Grain Boundary Scars and Spherical Crystallography. *Science* **2003**, *299*, 1716−1718.
(10) Bowick, M. J.; Giomi, L. Two-Dimensional Matter: Order, Curvature and Defects. *Adv. Phys.* **2009**, *58*, 449−563.
(11) Funkhouser, C. M.; Sknepnek, R.; Olvera de la Cruz, M. Topological Defects in the Buckling of Elastic Membranes. *Soft Matter* **2013**, *9*, 60−68.
(12) Bowick, M. J.; Sknepnek, R. Pathways to Faceting of Vesicles. *Soft Matter* **2013**, *9*, 8088−8095.
(13) Lidmar, J.; Mirny, L.; Nelson, D. R. Virus Shapes and Buckling Transitions in Spherical Shells. *Phys. Rev. E* **2003**, *68*, No. 051910.
(14) Guttman, S.; Kesselman, E.; Jacob, A.; Marin, O.; Danino, D.; Deutsch, M.; Sloutskin, E. Nanostructures, Faceting, and Splitting in Nanoliter to Yoctoliter Liquid Droplets. *Nano Lett.* **2019**, *19*, 3161−3168.
(15) García-Aguilar, I.; Fonda, P.; Sloutskin, E.; Giomi, L. Faceting and Flattening of Emulsion Droplets: A Mechanical Model. *Phys. Rev. Lett.* **2021**, *126*, No. 038001.
(16) Marin, O.; Tkachev, M.; Sloutskin, E.; Deutsch, M. Polyhedral Liquid Droplets: Recent Advances in Elucidation and Application. *Curr. Opin. Colloid Interface Sci.* **2020**, *49*, 107−117.
(17) Lesov, I.; Valkova, Z.; Vassileva, E.; Georgiev, G. S.; Ruseva, K.; Simeonov, M.; Tcholakova, S.; Denkov, N. D.; Smoukov, S. K. Bottom-Up Synthesis of Polymeric Micro- and Nanoparticles with Regular Anisotropic Shapes. *Macromolecules* **2018**, *51*, 7456−7462.
(18) Marin, O.; Alesker, M.; Guttman, S.; Gershinsky, G.; Edri, E.; Shpaisman, H.; Guerra, R. E.; Zitoun, D.; Deutsch, M.; Sloutskin, E. Self-Faceting of Emulsion Droplets as a Route to Solid Icosahedra and Other Polyhedra. *J. Colloid Interface Sci.* **2019**, *538*, 541−545.
(19) Marin, O.; Deutsch, M.; Zitoun, D.; Sloutskin, E. Nanoparticle Positioning on Liquid and Polymerized Faceted Droplets. *J. Phys. Chem. C* **2019**, *123*, 28192−28200.
(20) Vignati, E.; Piazza, R.; Lockhart, T. P. Pickering Emulsions: Interfacial Tension, Colloidal Layer Morphology, and Trapped-Particle Motion. *Langmuir* **2003**, *19*, 6650−6656.
(21) Thijssen, J. H. J.; Schofield, A. B.; Clegg, P. S. How Do (Fluorescent) Surfactants Affect Particle-Stabilized Emulsions? *Soft Matter* **2011**, *7*, 7965−7968.
(22) Hu, Z.; Patten, T.; Pelton, R.; Cranston, E. D. Synergistic Stabilization of Emulsions and Emulsion Gels with Water-Soluble Polymers and Cellulose Nanocrystals. *ACS Sustain. Chem. Eng.* **2015**, *3*, 1023−1031.
(23) Hollestelle, C.; Michon, C.; Fayolle, N.; Huc-Mathis, D. Co-Stabilization Mechanisms of Solid Particles and Soluble Compounds in Hybrid Pickering Emulsions Stabilized by Unrefined Apple Pomace Powder. *Food Hydrocoll.* **2024**, *146*, No. 109184.
(24) Xu, M.; Zhang, W.; Jiang, J.; Pei, X.; Zhu, H.; Cui, Z.; Binks, B. P. Transition between a Pickering Emulsion and an Oil-in-Dispersion Emulsion Costabilized by Alumina Nanoparticles and a Cationic Surfactant. *Langmuir* **2020**, *36*, 15543−15551.
(25) Liber, S. R.; Butenko, A. V.; Caspi, M.; Guttman, S.; Schultz, M.; Schofield, A. B.; Deutsch, M.; Sloutskin, E. Precise Self-Positioning of Colloidal Particles on Liquid Emulsion Droplets. *Langmuir* **2019**, *35*, 13053−13061.
(26) Cholakova, D.; Valkova, Z.; Tcholakova, S.; Denkov, N.; Binks, B. P. Spontaneous Particle Desorption and 'Gorgon' Drop Formation from Particle-Armored Oil Drops upon Cooling. *Soft Matter* **2020**, *16*, 2480−2496.
(27) Velev, O. D.; Furusawa, K.; Nagayama, K. Assembly of Latex Particles by Using Emulsion Droplets as Templates. 1. Microstructured Hollow Spheres. *Langmuir* **1996**, *12*, 2374−2384.
(28) Honaryar, H.; Amirfattahi, S.; Niroobakhsh, Z. Associative Liquid-In-Liquid 3D Printing Techniques for Freeform Fabrication of Soft Matter. *Small* **2023**, *19*, No. 2206524.
(29) Lei, D.; Yu, Y.; Kuang, Y.-L.; Liu, J.; Krauss, R. M.; Ren, G. Single-Molecule 3D Imaging of Human Plasma Intermediate-Density Lipoproteins Reveals a Polyhedral Structure. *BBA - Mol. Cell Biol. L.* **2019**, *1864*, 260−270.
(30) Cholakova, D.; Denkov, N.; Tcholakova, S.; Lesov, I.; Smoukov, S. K. Control of Drop Shape Transformations in Cooled Emulsions. *Adv. Coll. Interface Sci.* **2016**, *235*, 90−107.
(31) Liber, S. R.; Indech, G.; van der Wee, E. B.; Butenko, A. V.; Kodger, T. E.; Lu, P. J.; Schofield, A. B.; Weitz, D. A.; van Blaaderen, A.; Sloutskin, E. Axial Confocal Tomography of Capillary-Contained Colloidal Structures. *Langmuir* **2017**, *33*, 13343−13349.
(32) Li, S.; Zandi, R.; Travesset, A.; Grason, G. M. Ground States of Crystalline Caps: Generalized Jellium on Curved Space. *Phys. Rev. Lett.* **2019**, *123*, No. 145501.
(33) Irvine, W.; Vitelli, V.; Chaikin, P. M. Pleats in Crystals on Curved Surfaces. *Nature* **2010**, *468*, 947−951.
(34) Antl, L.; Goodwin, J.; Hill, R.; Ottewill, R.; Owens, S.; Papworth, S.; Waters, J. The Preparation of Poly(methyl methacrylate) Latices in Non-Aqueous Media. *Colloids Surf.* **1986**, *17*, 67−78.
(35) Davidyan, S.; Matoz-Fernandez, D. A.; Butenko, A. V.; García-Aguilar, I.; Giomi, L.; Sloutskin, E. Controlling Clouds-to-Scars Dislocations' Transitions on Spherical Crystal Shells. *Phys. Rev. Res.* **2024**, *6*, No. 043098.
(36) Sloutskin, E.; Sapir, Z.; Bain, C. D.; Lei, Q.; Wilkinson, K. M.; Tamam, L.; Deutsch, M.; Ocko, B. M. Wetting, Mixing, and Phase Transitions in Langmuir-Gibbs Films. *Phys. Rev. Lett.* **2007**, *99*, No. 136102.
(37) Aveyard, R.; Binks, B. P.; Clark, S.; Mead, J. Interfacial Tension Minima in Oil−Water−Surfactant Systems. Behaviour of Alkane−Aqueous NaCl Systems Containing Aerosol OT. *J. Chem. Soc., Faraday Trans.* **1986**, *1* (82), 125−142.
(38) Manoharan, V. N.; Elsesser, M. T.; Pine, D. J. Dense Packing and Symmetry in Small Clusters of Microspheres. *Science* **2003**, *301*, 483−487.
(39) Janai, E.; Butenko, A. V.; Schofield, A. B.; Sloutskin, E. Periodic Buckling and Grain Boundary Slips in a Colloidal Model of Solid Friction. *Soft Matter* **2019**, *15*, 5227−5233.
(40) Janai, E.; Butenko, A. V.; Schofield, A. B.; Sloutskin, E. Direct Imaging of Vibrations in Colloidal Crystals: In Equilibrium and in a Steady Drift. *J. Phys. Chem. C* **2016**, *120*, 8392−8398.
(41) Kanai, T.; Boon, N.; Lu, P. J.; Sloutskin, E.; Schofield, A. B.; Smallenburg, F.; van Roij, R.; Dijkstra, M.; Weitz, D. A. Crystallization and Reentrant Melting of Charged Colloids in Nonpolar Solvents. *Phys. Rev. E* **2015**, *91*, No. 030301.

https://doi.org/10.1021/acsnano.4c13476
ACS Nano XXXX, XXX, XXX−XXX

(42) Guttman, S.; Sapir, Z.; Ocko, B. M.; Deutsch, M.; Sloutskin, E. Temperature-Tuned Faceting and Shape-Changes in Liquid Alkane Droplets. *Langmuir* **2017**, *33*, 1305−1314.
(43) Buttinoni, I.; Dullens, R. P. A. Mechanical Properties of Colloidal Crystals at Fluid Interfaces. *J. Phys. Mater.* **2021**, *4*, No. 025001.
(44) Roke, S.; Berg, O.; Buitenhuis, J.; van Blaaderen, A.; Bonn, M. Surface Molecular View of Colloidal Gelation. *Proc. Natl. Acad. Sci. U.S.A.* **2006**, *103*, 13310−13314.
(45) Tamam, L.; Pontoni, D.; Sapir, Z.; Yefet, S.; Sloutskin, E.; Ocko, B. M.; Reichert, H.; Deutsch, M. Modification of Deeply Buried Hydrophobic Interfaces by Ionic Surfactants. *Proc. Natl. Acad. Sci. U.S.A.* **2011**, *108*, 5522−5525.
(46) Elbers, N. A.; van der Hoeven, J. E. S.; de Winter, D. A. M.; Schneijdenberg, C. T. W. M.; van der Linden, M. N.; Filion, L.; van Blaaderen, A. Repulsive Van der Waals Forces Enable Pickering Emulsions with Non-Touching Colloids. *Soft Matter* **2016**, *12*, 7265−7272.
(47) Leunissen, M. E.; van Blaaderen, A.; Hollingsworth, A. D.; Sullivan, M. T.; Chaikin, P. M. Electrostatics at the Oil−Water Interface, Stability, and Order in Emulsions and Colloids. *Proc. Natl. Acad. Sci. U.S.A.* **2007**, *104*, 2585−2590.
(48) Matoz-Fernandez, D. A.; Li, S.; de la Cruz, M. O.; Sknepnek, R. PyMembrane: A Flexible Framework for Efficient Simulations of Elastic and Liquid Membranes. *arXiv preprint arXiv:2308.12754*, 2023.
(49) Vernizzi, G.; Sknepnek, R.; de la Cruz, M. O. Platonic and Archimedean Geometries in Multicomponent Elastic Membranes. *Proc. Natl. Acad. Sci. U. S. A.* **2011**, *108*, 4292−4296.
(50) Sknepnek, R.; Vernizzi, G.; Olvera de la Cruz, M. Buckling of Multicomponent Elastic Shells with Line Tension. *Soft Matter* **2012**, *8*, 636−644.
(51) Budinski-Petković, L.; Kozmidis-Luburić, U. Random Sequential Adsorption on a Triangular Lattice. *Phys. Rev. E* **1997**, *56*, 6904−6908.
(52) Wang, D.; Dasgupta, T.; van der Wee, E. B.; Zanaga, D.; Altantzis, T.; Wu, Y.; Coli, G. M.; Murray, C. B.; Bals, S.; Dijkstra, M.; et al. Binary Icosahedral Clusters of Hard Spheres in Spherical Confinement. *Nat. Phys.* **2021**, *17*, 128−134.
(53) Shool, L.; Butenko, A. V.; Liber, S. R.; Rabin, Y.; Sloutskin, E. Anomalous Temperature-Controlled Concave-Convex Switching of Curved Oil-Water Menisci. *J. Phys. Chem. Lett.* **2021**, *12*, 6834−6839.
(54) Hsu, E.; Lee, D.; Sloutskin, E. Non-Classical Euler Buckling and Brazier Instability in Cylindrical Liquid Droplets. *Nano Lett.* **2024**, *24*, 8717−8722.
(55) Bradley, L. C.; Stebe, K. J.; Lee, D. Clickable Janus Particles. *J. Am. Chem. Soc.* **2016**, *138*, 11437−11440.
(56) Cholakova, D.; Lisicki, M.; Smoukov, S. K.; Tcholakova, S.; Lin, E. E.; Chen, J.; De Canio, G.; Lauga, E.; Denkov, N. Rechargeable Self-Assembled Droplet Microswimmers Driven by Surface Phase Transitions. *Nat. Phys.* **2021**, *17*, 1050−1055.
(57) Hallatschek, O.; Datta, S. S.; Drescher, K.; Dunkel, J.; Elgeti, J.; Waclaw, B.; Wingreen, N. S. Proliferating Active Matter. *Nat. Rev. Phys.* **2023**, *5*, 407−419.
(58) Tcholakova, S.; Valkova, Z.; Cholakova, D.; Vinarov, Z.; Lesov, I.; Denkov, N.; Smoukov, S. K. Efficient Self-Emulsification via Cooling-Heating Cycles. *Nat. Commun.* **2017**, *8*, No. 15012.
(59) Tu, F.; Lee, D. Shape-Changing and Amphiphilicity-Reversing Janus Particles with pH-Responsive Surfactant Properties. *J. Am. Chem. Soc.* **2014**, *136*, 9999−10006.
(60) Hacmon, S.; Liber, S. R.; Shool, L.; Butenko, A. V.; Atkins, A.; Sloutskin, E. Magic Numbers in Self-Faceting of Alcohol-Doped Emulsion Droplets. *Small* **2023**, *19*, No. 2301637.
(61) Nanikashvili, P. M.; Butenko, A. V.; Deutsch, M.; Lee, D.; Sloutskin, E. Salt-Induced Stability and Modified Interfacial Energetics in Self-Faceting Emulsion Droplets. *J. Colloid Interface Sci.* **2022**, *621*, 131−138.
(62) Liber, S. R.; Marin, O.; Butenko, A. V.; Ron, R.; Shool, L.; Salomon, A.; Deutsch, M.; Sloutskin, E. Polyhedral Water Droplets: Shape Transitions and Mechanism. *J. Am. Chem. Soc.* **2020**, *142*, 8672−8678.

https://doi.org/10.1021/acsnano.4c13476
ACS Nano XXXX, XXX, XXX−XXX